FAST OPTIMAL DESIGN OF SEMICONDUCTOR DEVICES

MARTIN BURGER* AND RENÉ PINNAU†

Abstract. This paper presents a new approach to the design of semiconductor devices, which leads to fast optimization methods whose numerical effort is of the same order as a single forward simulation of the underlying model, the *stationary drift-diffusion system*. The design goal we investigate is to increase the outflow current on a contact for fixed applied voltage, the natural design variable is the doping profile.

By reinterpreting the doping profile as a state variable and the electrostatic potential as the new design variable, we obtain a simpler optimization problem, whose Karush-Kuhn-Tucker conditions partially decouple. This property allows to construct efficient iterative optimization algorithms, which avoid to solve the fully coupled drift-diffusion system, but only need solves of the continuity equations and their adjoints. The efficiency and success of the new approach is demonstrated in several numerical examples.

Key words. Semiconductor design, drift-diffusion, optimal control, dopant profiling.

AMS subject classifications. 35J50, 49J20, 49K20.

1. Introduction.

Optimal design and characterization of semiconductor devices is a field of growing interest in the recent years, in the engineering (cf. e.g. [5, 6, 13, 14, 18, 20, 21, 22]) as well as in the applied mathematics community (cf. e.g. [2, 3, 7, 8, 9, 10, 11]). A major objective in the optimal design of devices is to improve the current flow over some contact by modifying the device doping profile, which enters as a source term in the mathematical model for semiconductor devices used, the so-called *drift-diffusion system*.

The stationary drift-diffusion system in physical variables consists of nonlinear elliptic equations for the electrostatic potential V, the electron density n, and the hole density p:

$$\begin{aligned} \operatorname{div}(\epsilon_s \nabla V) &= q(n-p-C) && \text{in } \Omega, \\ \operatorname{div}(D_n \nabla n - \mu_n n \nabla V) &= 0 && \text{in } \Omega, \\ \operatorname{div}(D_p \nabla p + \mu_p p \nabla V) &= 0 && \text{in } \Omega, \end{aligned}$$

where ϵ_s denotes the semiconductor permittivity, q the elementary charge, μ_n and μ_p are the electron and hole mobilities, D_n and D_p are the electron and hole diffusion coefficients, respectively. This is system is supplemented by homogeneous Neumann boundary conditions on a part $\partial\Omega_N$ of the boundary, modelling the insulating parts of the boundary, and Dirichlet conditions on the remaining part, which models the Ohmic contacts of the device:

$$\begin{aligned} V(x) &= V_D(x) = U(x) + V_{bi}(x) = U(x) + U_T \ln\left(\frac{n_D(x)}{n_i}\right) && \text{on } \partial\Omega_D, \\ n(x) &= n_D(x) = \frac{1}{2}\left(C(x) + \sqrt{C(x)^2 + 4n_i^2}\right) && \text{on } \partial\Omega_D, \\ p(x) &= p_D(x) = \frac{1}{2}\left(-C(x) + \sqrt{C(x)^2 + 4n_i^2}\right) && \text{on } \partial\Omega_D. \end{aligned}$$

*Institut für Industriemathematik, Johannes Kepler Universität Linz, Altenbergerstr. 69, A-4040 Linz, Austria (`burger@indmath.uni-linz.ac.at`)

†Fachbereich Mathematik, Technische Universität Darmstadt, Schlossgartenstr. 7, D-64289 Darmstadt, Germany (`pinnau@mathematik.tu-darmstadt.de`)

Here n_i is the intrinsic density, U_T the thermal voltage and U is the applied biasing voltage.

Under usual conditions, the mobilities and diffusion coefficients are related by Einstein's relation, i.e., $D_{n/p} = \mu_{n/p} U_T$. which enables the transformation into the so-called *Slotboom variables* [19] defined by

$$n = n_i e^{V/U_T} u, \qquad p = n_i e^{V/U_T} v. \tag{1.1}$$

The assumptions that ϵ_s and q are constant allows for the choice of an appropriate scaling yielding the system

$$\lambda^2 \Delta V = (e^V u - e^{-V} v) - C \qquad \text{in } \Omega \tag{1.2}$$

$$\text{div}\left(\mu_n e^V \nabla u\right) = 0 \qquad \text{in } \Omega \tag{1.3}$$

$$\text{div}\left(\mu_p e^{-V} \nabla v\right) = 0 \qquad \text{in } \Omega \tag{1.4}$$

where $\lambda^2 = (\epsilon_s U_T)/(q\, C_{max}\, L^2)$ is the scaled Debye length of the device (for details see e.g. [16]). The Dirichlet boundary conditions can be written as

$$V = V_D = U + V_{bi} \qquad \text{on } \partial\Omega_D \tag{1.5}$$

$$u = u_D \qquad \text{on } \partial\Omega_D \tag{1.6}$$

$$v = v_D \qquad \text{on } \partial\Omega_D \tag{1.7}$$

where u_D and v_D are the transformations of n_D and v_D under (1.1). On the remaining part $\partial\Omega_N = \partial\Omega \setminus \partial\Omega_D$, the homogeneous Neumann conditions can be formulated on J_n and J_p, where J_n and J_p are the electron and hole current densities, which are related to the Slotboom variables by

$$J_n = \mu_n e^v \nabla u, \qquad J_p = -\mu_p e^{-V} \nabla v. \tag{1.8}$$

Hence, we have

$$\frac{\partial V}{\partial \nu} = 0 \qquad \text{on } \partial\Omega_N \tag{1.9}$$

$$\frac{\partial u}{\partial \nu} = 0 \qquad \text{on } \partial\Omega_N \tag{1.10}$$

$$\frac{\partial v}{\partial \nu} = 0 \qquad \text{on } \partial\Omega_N \tag{1.11}$$

Throughout the whole paper, we shall assume that all Dirichlet boundary values V_D, u_D, and v_D, are bounded in $H^{\frac{1}{2}}(\Omega) \cap L^\infty(\Omega)$, which is the basis for an existence proof of the drift-diffusion system in $(H^1(\Omega) \cap L^\infty(\Omega))^3$ [16].

The objective of the optimization, the current flow over a contact Γ, is given by

$$I = \int_\Gamma J.d\nu = \int_\Gamma (J_n + J_p).d\nu. \tag{1.12}$$

An optimal control approach to the optimization of a functional related to the current density J or the current flow I was investigated in [10, 11], where the drift-diffusion system (1.2)-(1.11) was interpreted as an equation constraint determining the state (V, u, v). Consequently, a penalty term related to the control variable C was added to the objective in order to stabilize the system. To the penalizing problem, an iterative algorithm was applied, which as usual needed solutions of the drift-diffusion system and some adjoint system in each iteration. In this paper we investigate a completely different approach, namely we reinterpret the potential V as the design variable and the doping profile C as a state variable. For given V satisfying appropriate boundary conditions, it is easy to show that the drift-diffusion system has a unique solution (u, v, C) and moreover, the partial differential equations (1.2)-(1.4) have a simple triangular structure in the new state variables. Corresponding to our interpretation of state and design variables we add a penalty term corresponding to V to the objective functional in order to stabilize the problem. As we shall see below, this yields a reasonably simple optimality system, from which a fast optimization algorithm can be constructed.

For the sake of simplicity and shortness of presentation we assume that $\mu_n = \mu_p = 1$, but analogous reasoning is possible for general mobilities, even for energy dependent ones. Moreover we ignore recombination-generation terms [19], noting that they could be incorporated into our analysis with only few modifications.

The paper is organized as follows: in Section 2 we review the current state in semiconductor design and introduce our new optimization approach. Some basic analysis of the optimization problem under investigation (such as existence of solutions and first-order optimality) is provided in Section 3. Section 4 is devoted to the iterative solution of the optimal design problem, and in particular an efficient method based on a lower diagonal approximation of the Karush-Kuhn-Tucker system is introduced. Numerical results for some diodes and a MESFET device are presented in Section 5, and finally we give some conclusions in Section 6.

2. Optimal Design of Semiconductor Devices. In the following we discuss some basic problems in optimal semiconductor design and present a new approach for optimization problems at a single applied voltage.

Although the optimal design of semiconductor devices is of major importance in practical applications, the first systematic approaches to such optimization problems have been carried out only in the last few years (cf. [10, 11, 18, 20, 21, 22]). Probably one of the main reason for this late development are the computational difficulties and the complexity of such optimization problem. Even the numerical solution of the drift-diffusion system itself is not a simple task, and an optimization based on the drift-diffusion model therefore becomes quite involved. In the first optimization approaches to this problem, gradient-type methods have been used, with gradient evaluations either by finite differencing (cf. [18, 20, 21, 22]) or by an adjoint method (cf. [10, 11]). Both approaches resulted in a very high numerical effort due to a large number of iterations needed. E.g., by finite differencing around 4000 direct solutions of the drift-diffusion system were needed for the optimization of a MOSFET device, at a rather coarse discretization of the doping profile with 62 design parameters (cf. [18]). The adjoint approach, used in [11] for the minimization of a functional of the form

$$Q_\beta(C) := Q(n(C), p(C), V(C)) + \frac{\beta}{2}\|C - C^*\|^2 \to \min_C, \tag{2.1}$$

reduces the number of nonlinear solves, and adds few solves of an adjoint linear system. This reduces the numerical effort, but causes the need for an accurate discretization and numerical solution of the adjoint system, which is not well investigated so far.

We use a different approach, based on exchanging the interpretations of control and state between C and V. We interpret the potential V as the design variable and interpret the Poisson equation (1.2) as a state equation for the doping profile C. Consequently, we introduce a penalty dependent on $V - V^*$ rather than on $C - C^*$. As the initial guess V^* we use the one obtained from the solution of the drift-diffusion system with doping profile C^*. Since the Laplacian of $V - V^*$ is needed for the evaluation of $C - C^*$, it seems natural to use a penalty term dependent on

$$W := \Delta(V - V^*), \tag{2.2}$$

i.e., we minimize the functional

$$Q_\epsilon(u, u, V, W) := Q(u, v, V) + \frac{\epsilon}{2} \int_\Omega |W(x)|^2 \, dx, \tag{2.3}$$

subject to (2.2) and the drift-diffusion system. In order to ensure that C does not change its boundary values, W must satisfy homogeneous boundary conditions on $\partial\Omega_D$, on the remaining boundary we may use any homogeneous boundary condition. For simplicity we will carry out our analysis for

$$W = 0 \qquad \text{on } \partial\Omega, \tag{2.4}$$

in a numerical test (cf. Section 5.3) we will use the boundary condition $W = 0$ on $\partial\Omega_D$ and $\frac{\partial W}{\partial \nu} = 0$ on $\partial\Omega_N$, which permits a similar analysis.

Of particular importance are functionals Q, which depend only on the values the outflow current density on some contact Γ, i.e.,

$$Q(u, v, V) = R(J.\nu|_\Gamma) = R\left((e^V \frac{\partial u}{\partial \nu} - e^{-V} \frac{\partial u}{\partial \nu})|_\Gamma \right). \tag{2.5}$$

In [11], the functional under investigation was

$$R(J.\nu|_\Gamma) = \frac{1}{2} \|(J - J^*).\nu\|^2_{H^{-\frac{1}{2}}(\Gamma)}, \tag{2.6}$$

corresponding to the objective of finding an outflow current density $J.\nu$ close to a desired density $J^*.\nu$. Since in most practical applications, one is rather interested in the total current flow on a contact, we rather consider the functional

$$R(J.\nu|_\Gamma) = \frac{1}{2} \left| \int_\Gamma J.d\nu - I^* \right|^2 \tag{2.7}$$

(for some desired current flow I^*) as the motivation for the analysis in this paper and also use it for our numerical tests. We also note that for one-dimensional diodes, which have been investigated in [11] and will also be used for some of our numerical tests, the above two functionals are equivalent, since the geometry of a contact corresponds to a boundary point of an interval.

3. Analysis of the Optimization Problem. In the following we provide some analysis of the optimization problem

$$Q_\epsilon(u, v, V, W) \to \min_{(n,p,V,W) \in \mathcal{D}_{ad}}, \tag{3.1}$$

with the admissible domain

$$\mathcal{D}_{ad} := \{(u, v, V, W) \in H^1(\Omega)^2 \times (H^1(\Omega) \cap L^\infty(\Omega)) \times L^2(\Omega) \\ \text{satisfying (1.3)-(1.11), (2.2) }\}.$$

We shall investigate the existence of minima as well as a derivation of the Karush-Kuhn-Tucker conditions, which allows to deduce further regularity of minimizers.

3.1. Existence of a Minimum. We start our analysis with a basic result on the existence of minima, for which we need two fundamental properties, namely the weak lower semicontinuity of the objective functional and the weak closedness of the admissible domain. Weak lower semicontinuity of Q_ϵ is obviously obtained in $H^1(\Omega)^3 \times L^2(\Omega)$, the weak closedness of $\mathcal{D}_{ad}$ is obtained if $\Delta(V - V^*)$ remains in $L^2(\Omega)$. This leads us to the following result:

THEOREM 3.1 (Existence). *Let $\epsilon > 0$. Then there exists a minimum*

$$(\overline{u}, \overline{v}, \overline{V}, \overline{W}) \in H^1(\Omega)^2 \times (H^1(\Omega) \cap L^\infty(\Omega)) \times L^2(\Omega). \tag{3.2}$$

of (3.1).

Proof. Suppose $(u^k, v^k, V^k, W^k)_{k\in\mathbb{N}}$ is a minimizing sequence, then we immediately may conclude that W^k is bounded in $L^2(\Omega)$ and thus, by standard elliptic regularity, $V^k - V^*$ is uniformly bounded in $H^2(\Omega) \hookrightarrow C(\overline{\Omega})$. Since the a-priori guess V^* is in $L^\infty(\Omega)$, we obtain uniform boundedness of V^k in $L^\infty(\Omega)$. Standard energy arguments for the elliptic equations (1.3) and (1.4) consequently yield the boundedness of u^k and v^k in $H^1(\Omega) \cap L^\infty(\Omega)$. Thus, we may extract a weakly converging subsequence $(u_{k_\ell}, v_{k_\ell}, V_{k_\ell}, W_{k_\ell})_{k_\ell\in\mathbb{N}} \in H^1(\Omega)^2 \times H^1(\Omega) \times L^2(\Omega)$, which also preserves the L^∞ bound (and such that $\Delta(V_{k_\ell} - V^*)$ converges weakly in $L^2(\Omega)$). The weak closedness of the admissible domain and the weak lower semicontinuity of the objective functional imply that the weak limit of this subsequence is a minimizer of (3.1). □

A direct consequence of the representation

$$C = C^* - \lambda^2 W + n - n^* - p + p^*$$

is the existence of a doping profile $C \in L^2(\Omega)$ such that (u, v, V) is a solution of the corresponding drift-diffusion system.

COROLLARY 3.2. *Let $\epsilon > 0$. Then there exists a minimum*

$$(\overline{u}, \overline{v}, \overline{V}, \overline{W}) \in H^1(\Omega)^2 \times (H^1(\Omega) \cap L^\infty(\Omega)) \times L^2(\Omega). \tag{3.3}$$

of (3.1), *and a doping profile $\overline{C} \in L^2(\Omega)$ such that $(\overline{u}, \overline{v}, \overline{V})$ is a weak solution of the drift-diffusion system* (1.2)–(1.11) *with $C = \overline{C}$.*

3.2. First-Order Optimality. In order to derive the first-order optimality conditions, we define the Lagrangian given by

$$\mathcal{L}(u, v, V, W; \mu_1, \mu_2, \mu_3) = Q_\epsilon(u, v, V, W) + \int_\Omega \left(e^V \nabla u . \nabla \mu_1 - e^{-V} \nabla v \nabla \mu_2\right) \, dx$$
$$+ \int_\Omega \left(\nabla(V - V^*) . \nabla \mu_3 + W \mu_3\right) \, dx. \tag{3.4}$$

One observes that the only nonlinear terms in the equation constraints (1.3) - (1.11), (2.2) are of the form $e^V \nabla u$ and $e^{-V} \nabla v$, and these are continuously Fréchet-differentiable in $\mathcal{D}_{ad}$ since $V \in H^1(\Omega) \cap L^\infty(\Omega)$ and $(u, v) \in H^1(\Omega)^2$. Hence, with little effort we obtain the following result:

PROPOSITION 3.3. *The Lagrangian $\mathcal{L}$ is continuously Fréchet-differentiable on $\mathcal{D}_{ad} \times H^1(\Omega)^3$.*

Each solution of the optimization problem is a saddle point of the Lagrangian, i.e., a solution of

$$\inf_{(u,v,V,W)} \sup_{(\mu_1,\mu_2,\mu_3)} \mathcal{L}(u, v, V, W; \mu_1, \mu_2, \mu_3). \tag{3.5}$$

For such saddle-points we can derive the Karush-Kuhn-Tucker conditions by computing the variations of the Lagrangian $\mathcal{L}$ with respect to all primal and dual variables, which all must vanish. The variations with respect to the dual variables just yield the equality constraints, while from the variation with respect to the primal variables we deduce that

$$0 = \frac{\partial}{\partial u} Q_\epsilon(u,v,V,W)\hat{u} + \int_\Omega \left(e^V \nabla\hat{u}.\nabla\mu_1\right) dx \tag{3.6}$$

$$0 = \frac{\partial}{\partial v} Q_\epsilon(u,v,V,W)\hat{v} - \int_\Omega \left(e^V \nabla\hat{v}.\nabla\mu_2\right) dx \tag{3.7}$$

$$0 = \frac{\partial}{\partial V} Q_\epsilon(u,v,V,W)\hat{V} + \int_\Omega \left(\hat{V}\left(e^V \nabla u.\nabla\mu_1 + e^{-V}\nabla v \nabla\mu_2\right) + \nabla\hat{V}.\nabla\mu_3\right) dx \tag{3.8}$$

$$0 = \int_\Omega \hat{W}(\epsilon W - \mu_3) dx, \tag{3.9}$$

holds for all variations $(\hat{u},\hat{v},\hat{V},\hat{W}) \in H^1(\Omega)^3 \times L^2(\Omega)$.

One observes that the so-called *adjoint equations* (3.6)-(3.8) have a simple triangular structure with respect to the Lagrangian variables. Thus, the problem of proving existence and uniqueness of Lagrangian variables $(\mu_1,\mu_2,\mu_3) \in H^1_{0,D}(\Omega)^3$ solving (3.6)-(3.8) for given primal variables (u,v,V), simplifies to analyzing subsequently three different variational problems, which turn out to be coercive in $H^1_{0,D}(\Omega)$. This yields another advantage of our approach with respect to the direct optimal control approach, where analyzing the adjoint problem is a difficult task, which is possible only close to thermal equilibrium (cf. [11]).

THEOREM 3.4. *Let $(u,v,V,W) \in \mathcal{D}_{ad}$ be given, then there exists a unique solution $(\mu_1,\mu_2,\mu_3) \in H^1_{0,D}(\Omega)^3$ of the variational problem* (3.6)-(3.8).

Proof. The variational problem (3.6) is of the form

$$A(\mu_3,\hat{u}) = \langle F,\hat{u}\rangle, \qquad \forall\ \hat{u} \in H^1_{0,D}(\Omega),$$

with a continuous linear functional F on $H^1_{0,D}(\Omega)$ and a coercive, continuous bilinear form

$$A(u,v) = \int_\Omega e^V \nabla u.\nabla v \ dx \quad \text{ on } H^1_{0,D}(\Omega)^2.$$

Thus, existence and uniqueness of μ_1 follows from the Lax-Milgram Theorem. Since we can apply analogous reasoning to (3.7), we also obtain the existence and uniqueness of μ_2. Since μ_1 and μ_2 are determined by (3.6), (3.7), we may consider them as a given right-hand side in (3.8). The latter is now a scalar problem for μ_3, whose well-posedness can again be shown by a straight-forward application of the Lax-Milgram Theorem. Note, that $L^2(\Omega) \hookrightarrow H^{-1}(\Omega)$. □

Our subsequent analysis will be carried out for the important case of Q being the outflow current functional (2.5). In this case, the derivative of the functional Q is given by

$$Q'(u,v,V)(\hat{u},\hat{v},\hat{V}) = R'(J.\nu|_\Gamma)\left(e^V \frac{\partial\hat{u}}{\partial\nu} - e^{-V}\frac{\partial\hat{v}}{\partial\nu} + (e^V\frac{\partial u}{\partial\nu} + e^{-V}\frac{\partial v}{\partial\nu})\hat{V}\right), \tag{3.10}$$

and noticing that $\hat{V} \in H^1_{0,D}(\Omega)$, we observe that the last term on the right-hand side vanishes. In the particular case of (2.7) the derivative simplifies to

$$Q'(u,v,V)(\hat{u},\hat{v},\hat{V}) = \left(\int_\Gamma J.d\nu - I^*\right)\int_\Gamma \left(e^V\frac{\partial\hat{u}}{\partial\nu} - e^{-V}\frac{\partial\hat{v}}{\partial\nu}\right) ds. \tag{3.11}$$

Due to the simple form of (3.9) it seems obvious to eliminate the Lagrangian variable $\mu_3 = \epsilon W$ and to rewrite (3.8) as

$$0 = \int_\Omega \left(\hat{V} \left(e^V \nabla u . \nabla \mu_1 + e^{-V} \nabla v \nabla \mu_2 \right) + \epsilon \nabla \hat{V} . \nabla W \right) dx. \tag{3.12}$$

This advices the interpretation of W as the design variable and (3.12) as the optimality condition corresponding to the minimization of the functional Q subject to the equality constraints (1.3), (1.4) for the state variables (u, v, V).

If we choose the Lagrangian variables μ_i, $i = 1, 2$ such that $\mu_i = 0$ only on $\partial\Omega_D \setminus \Gamma$ and $\mu_1 = \mu_2 = \eta$ on Γ for some real constant η, then we can derive a simple form of the optimality system. With this choice, the Lagrangian becomes

$$\begin{aligned} \mathcal{L}(u, v, V, W; \mu_1, \mu_2, \mu_3) = Q_\epsilon(u, v, V, W) + \int_\Omega \left(e^V \nabla u . \nabla \mu_1 - e^{-V} \nabla v \nabla \mu_2 \right) \, dx \\ + \int_\Omega \left(\nabla (V - V^*) . \nabla \mu_3 + W \mu_3 \right) \, dx - \eta \int_\Gamma J . d\nu, \end{aligned} \tag{3.13}$$

and the optimality with respect to u yields

$$\left(\int_\Gamma J . d\nu - I^* - \eta \right) \int_\Gamma \left(e^V \frac{\partial \hat{u}}{\partial \nu} \right) ds + \int_\Omega \left(e^V \nabla \hat{u} . \nabla \mu_1 \right) dx = 0. \tag{3.14}$$

With the choice $\eta = \int_\Gamma J . d\nu - I^*$, this reduces to the weak form corresponding to the elliptic partial differential equation

$$\text{div } \left(e^V \nabla \mu_1 \right) = 0 \qquad \text{in } \Omega, \tag{3.15}$$

subject to the boundary conditions

$$\mu_1 - \int_\Gamma J . d\nu + I^* = 0 \qquad \text{on } \Gamma \tag{3.16}$$

$$\mu_1 = 0 \qquad \text{on } \partial\Omega_D \setminus \Gamma \tag{3.17}$$

$$\frac{\partial \mu_1}{\partial \nu} = 0 \qquad \text{on } \partial\Omega_N. \tag{3.18}$$

Analogous reasoning yields the equation

$$\text{div } \left(e^{-V} \nabla \mu_2 \right) = 0 \qquad \text{in } \Omega, \tag{3.19}$$

subject to the same boundary conditions as for μ_1, determining the Lagrangian variable μ_2. Finally, we determine the optimality condition with respect to W can be rewritten as the equation

$$\epsilon \Delta W = e^V \nabla u . \nabla \mu_1 + e^{-V} \nabla v \nabla \mu_2 \qquad \text{in } \Omega, \tag{3.20}$$

subject to homogeneous Dirichlet conditions on $\partial\Omega_D$ and homogeneous Neumann conditions on $\partial\Omega_N$.

3.3. Regularity. In the following we use the Karush-Kuhn-Tucker system derived above, which has to be fulfilled by any solution of the optimal design problem, to prove additional regularity of minimizers. First of all, since W satisfies the Poisson equation (3.20) with right-hand side in $L^1(\Omega) \hookrightarrow H^{-1}(\Omega)$ and subject to the homogeneous boundary conditions (2.4), we may conclude that $W \in H^1(\Omega)$.

For the primal variables u and v, which satisfy the homogeneous elliptic equations (1.3) and (1.4), respectively, we can apply a standard maximum principle as in [16], which implies $u \in L^\infty(\Omega)$ and $v \in L^\infty(\Omega)$. Analogous reasoning can be applied to the dual variables μ_1 and μ_2, which solve the same elliptic equations as u and v, and whose Dirichlet boundary data are uniformly bounded, too (since μ_i is piecewise constant on $\partial\Omega_D$). Hence, we may conclude that $\mu_i \in L^\infty(\Omega)$, $i = 1, 2$. As a consequence of this type of regularity, we obtain that

$$\nabla(C - C^*) = -\lambda^2 \nabla W + e^V(u\nabla V + \nabla u) + e^{-V}(v\nabla V - \nabla v) \\ - e^{V^*}(u^*\nabla V^* + \nabla u^*) - e^{-V^*}(v^*\nabla V^* - \nabla v^*) \quad (3.21)$$

is bounded in $L^2(\Omega)$, since all the gradient terms on the right-hand side are in $L^2(\Omega)$ and the zero-order terms are in $L^\infty(\Omega)$. Thus, we have deduced the following type of regularity for minimizers:

THEOREM 3.5. *Let $(\overline{u}, \overline{v}, \overline{V}, \overline{W}) \in \mathcal{D}_{ad}$ be a minimizer of (3.1). Then,*

$$\overline{u} \in L^\infty(\Omega), \qquad \overline{v} \in L^\infty(\Omega), \qquad \overline{W} \in H^1(\Omega). \quad (3.22)$$

The Lagrangian variables $\overline{\mu}_i \in H^1(\Omega)$ associated to (1.3) and (1.4) satisfy

$$\overline{\mu}_1 \in L^\infty(\Omega), \qquad \overline{\mu}_2 \in L^\infty(\Omega). \quad (3.23)$$

Moreover, if $C^* \in H^1(\Omega)$, then the associated doping profile $\overline{C}$ (via (1.2)) satisfies $\overline{C} \in H^1(\Omega)$.

We finally give an interpretation of the optimality system with respect to the local regularity of the doping profile. If the initial doping profile C^* has a discontinuity (occurring typically at a p-n junction), then the according solution V^* is locally not C^2 across the junction, but (via standard regularity) on every open set not containing the junction. Since for a solution of the optimality system, $V - V^*$ satisfies a Poisson equation with homogeneous boundary data and a right-hand side W that we may expect to be smooth (W solves a Poisson equation itself), the solution $V - V^*$ should have higher regularity even across the discontinuity of the doping profile. Hence, the only source of lower regularity is contained in V^* and thus, its location must be the same for $V = (V - V^*) + V^*$.

4. A Fast Optimization Method. In the following we discuss a simple optimization method, which allows the design of semiconductor devices by solving decoupled elliptic partial differential equations only. For simplicity we consider the case of (2.5), (2.7) in the following, but an analogous approach is possible for different objective functionals, too.

We start by discussing the Lagrange-Newton iteration for the primal variables (u^k, v^k, V^k, W^k) and the dual variables (μ_1^k, μ_2^k), given by

$$\Delta V^k = \Delta V^* + W^k \quad (4.1)$$

$$\mathrm{div}\ (e^{V^{k-1}} \nabla u^k) = -\mathrm{div}\ (e^{V^{k-1}}(V^k - V_{k-1})\nabla u^{k-1}) \quad (4.2)$$

$$\mathrm{div}\ (e^{-V^{k-1}} \nabla v^k) = \mathrm{div}\ (e^{-V^{k-1}}(V^k - V_{k-1})\nabla u^{k-1}) \quad (4.3)$$

$$\mathrm{div}\ (e^{V^{k-1}} \nabla \mu_1^k) = -\mathrm{div}\ (e^{V^{k-1}}(V^k - V_{k-1})\nabla \mu_1^{k-1}) \quad (4.4)$$

$$\mathrm{div}\ (e^{-V^{k-1}} \nabla \mu_2^k) = \mathrm{div}\ (e^{-V^{k-1}}(V^k - V_{k-1})\nabla \mu_2^{k-1}) \quad (4.5)$$

$$-\epsilon W^k = -e^{V^{k-1}} \left((V^k \nabla u^{k-1} + \nabla u^k).\nabla \mu_1^{k-1} + \nabla u^{k-1}.\nabla \mu_1^k\right) \\ + e^{-V^{k-1}} \left((-V^k \nabla v^{k-1} + \nabla v^k).\nabla \mu_2^{k-1} + \nabla v^{k-1}.\nabla \mu_2^k\right), \quad (4.6)$$

subject to the boundary conditions (1.5)-(1.11) As for the solution of the drift-diffusion system, the full Lagrange-Newton method yields a sequence of systems of partial differential equations, which is in general non-elliptic due to the strong influence of first-order terms. As for the drift-diffusion system, we may expect the numerical solution of this system to be a difficult task, in particular for large applied voltages. Moreover, the advantage of our optimization approach, namely the partial decoupling into scalar elliptic partial differential equations, is lost by using this Newton-type approach.

Therefore it seems favourable to use a different iterative method for the solution of the optimality system. Using a lower triangular approximation of the optimality system, we first solve equation (2.2) with given W for the potential V, and subsequently the continuity equations (1.3), (1.4) with given potential V for u and v. With given potential and given u and v, we solve the adjoint equations (3.15), (3.19) to obtain the Lagrangian variables μ_1 and μ_2. Finally, we can perform a gradient step with respect to the design variable W using the optimality equation (3.20). Due to the simple structure of this equation, it seems reasonable to discretize the Laplace term in an implicit way and thus, to solve

$$-\epsilon W + \tau W = \tau W^* - e^V \nabla u . \nabla \mu_1 + e^{-V} \nabla v \nabla \mu_2, \tag{4.7}$$

for an appropriately chosen damping parameter τ, where W^* is the old value of W. All together, we can write this iteration as

$$\begin{aligned}
\Delta V^k &= \Delta V^* + W^{k-1} && (4.8)\\
\text{div } (e^{V^k} \nabla u^k) &= 0 && (4.9)\\
\text{div } (e^{-V^k} \nabla v^k) &= 0 && (4.10)\\
\text{div } (e^{V^k} \nabla \mu_1^k) &= 0 && (4.11)\\
\text{div } (e^{-V^k} \nabla \mu_2^k) &= 0 && (4.12)\\
-\epsilon W^k + \tau W^k &= \tau W^{k-1} - e^{V^k} \nabla u^k . \nabla \mu_1^k + e^{-V^k} \nabla v^k \nabla \mu_2^k, && (4.13)
\end{aligned}$$

subject to the above boundary conditions. The only coupling in the boundary conditions occurs in the condition $\mu_i = \int_\Gamma J^k . d\nu$, but also there we can use the previously computed values for u^k and v^k to obtain J^k. The corresponding value of the doping profile can be computed independently by

$$C^k - C^* = -\lambda^2 W^k + n^k - n^* - p^k + p^*, \tag{4.14}$$

where $n^k = e^{V^k} u^k$ and $p^k = e^{-V^k} v^k$.

5. Numerical Examples. In the following we report numerical results for three different examples, two bipolar diodes and a unipolar MESFET device. For all the numerical experiments we use the physical parameters for silicon as given in Table 5.1, with a standard forward-bias scaling of the variables (cf. [16]). The objective functional is given by (2.5), (2.7). All the numerical examples have been implemented within the software system MATLAB.

5.1. PN-Diode. Our first example is a pn-diode, with the domain Ω scaled to the unit interval $(0, 1)$. The pn-diode is characterized by a doping profile which has exactly one positive and one negative region; we choose one of the simplest possibilities for the (scaled) initial doping profile, namely a function jumping almost abruptly from

Parameter	Physical Meaning	Numerical Value
q	elementary charge	$1.6{\cdot}10^{-19}$ As
n_i	intrinsic density	10^{10} cm^{-3}
ϵ_S	permittivity constant	10^{-12} As V^{-1}s^{-1}
μ_0	low field mobility	$1.5{\cdot}10^{3}$ cm^{2}V^{-1}s^{-1}
U_T	thermal voltage at $T = 300$K	0.0259 V

TABLE 5.1
Physical parameters for silicon.

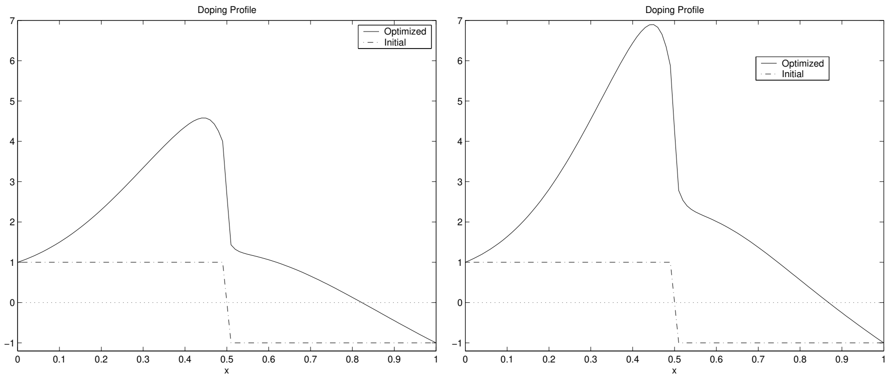

FIG. 5.1. *Initial (dash-dotted) and optimized (solid) doping profile in Example 5.1, for $\epsilon = 10^{-2}$ (left) and $\epsilon = 10^{-3}$ (right).*

the value 1 to -1 at the junction. This initial profile is shown as the dash-dotted function in Figure 5.1. The Debye length in this experiment is given by $\lambda^2 = 10^{-3}$ and the value of the applied voltage is $U = 10U_T = 0.259$. The optimization objective is to increase the current flow (i.e., the current flow density, which is constant in the domain since $J_x = 0$) by 50%, and consequently we chose

$$I^* = 1.5 \cdot \int_\Gamma J_0.d\nu, \tag{5.1}$$

where $\Gamma = \{0\}$ and J_0 is the current flow density obtained with the initial doping.

For the numerical solution of the drift-diffusion system and the linear elliptic equations arising during the iterative solution of the optimization problem in this example (as well as the following one) we use an exponentially fitted scheme of Scharfetter-Gummel type (cf. [4]), the fineness of the uniform spatial grid is given by $h = 10^{-2}$. For the discretization of all variables involved $(C, V, W, n, p, \mu_1, \mu_2)$ we use piecewise linear finite elements, the drift-diffusion system with given initial doping profile is solved using Newton's method and voltage continuation to obtain the initial value of the potential (cf. [17]).

The numerical results have been performed for several values of ϵ, with the result that most changes appeared for ϵ between 10^{-3} and 10^{-2}, so we plot the results for these two values in the Figures 5.1 - (note that for large values of ϵ the penalty does not allow enough change to the initial configuration, while for small values the observation tends to be almost zero in our case so that the further change in the solution is negligible). Figure 5.1 shows the optimized doping profiles (solid) in both cases compared to the initial one (dash-dotted). The dashed line is the coordinate axis

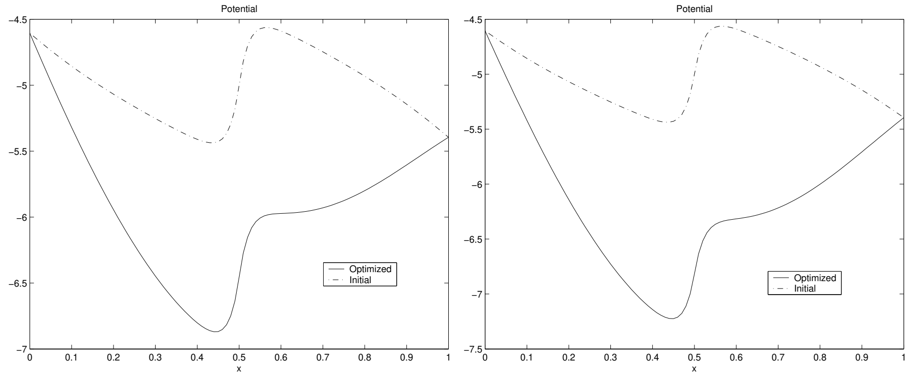

FIG. 5.2. *Initial (dash-dotted) and optimized (solid) potential in Example 5.1, for* $\epsilon = 10^{-2}$ *(left) and* $\epsilon = 10^{-3}$ *(right).*

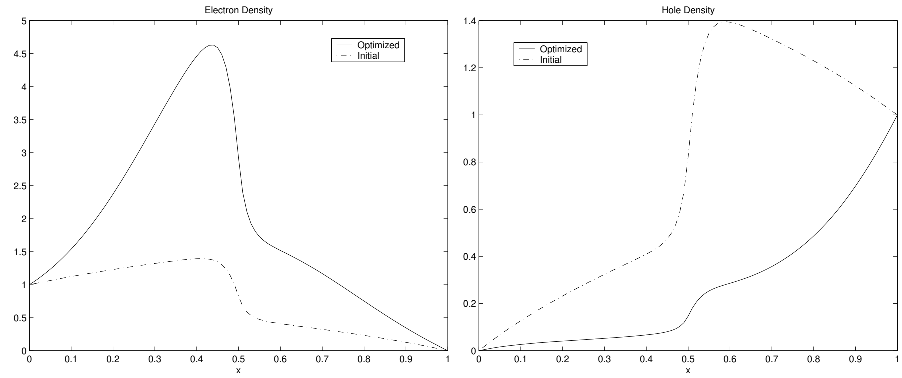

FIG. 5.3. *Initial (dash-dotted) and optimized (solid) electron (left) and hole density (right) in Example 5.1, for* $\epsilon = 10^{-3}$.

for x, its cut with the doping profile marks the pn-junction. One observes that the optimized doping profiles have similar shape for both values of ϵ, but the magnitude of the doping in the n-region grows with decreasing ϵ. In both cases the n-region grows on expense of the p-region, i.e., the pn-junction moves right and the value of C is larger than the initial one in the whole domain. Moreover, the doping profile remains steep around the center point $x = 0.5$, which numerically confirms the result obtained from the analysis of the optimality system.

An analogous effect happens with the potential V, which is the actual design variable in our approach, and with the electron and hole densities, i.e., the shape changes strongly compared to the initial one for $\epsilon = 10^{-2}$ and if we decrease the value of ϵ the resulting current flow can be forced to be closer to the desired one only by a change in magnitude. The resulting potentials for both values compared to the initial ones are shown in Figure 5.1. The electron and hole densities are shown in Figure 5.3 for the value of $\epsilon = 10^{-3}$.

Finally, we illustrate of the behaviour of objective functional, observation and of the penalizing energy term in the left plot of Figure 5.4, and the change in the current-voltage characteristic in the right plot (both for $\epsilon = 10^{-3}$). Not surprisingly, the objective functional and observation are reduced in few iterations, while the energy

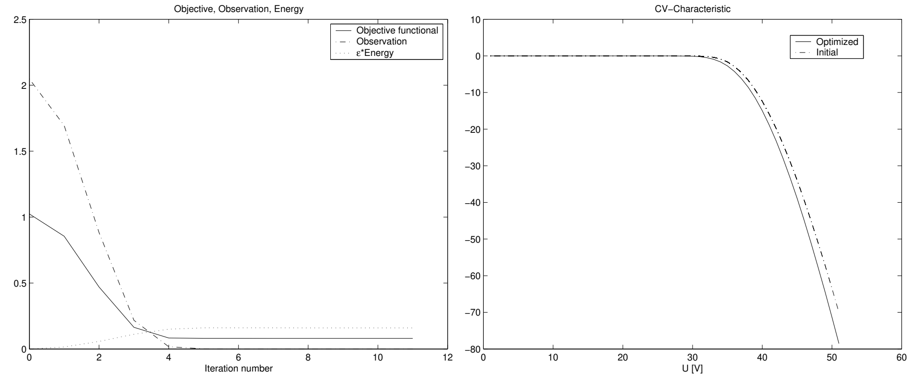

FIG. 5.4. *Evolution of the objective functional (solid), observation (dash-dotted) and energy (dotted) in Example 5.1 (left), and current-voltage characteristic, for $\epsilon = 10^{-3}$.*

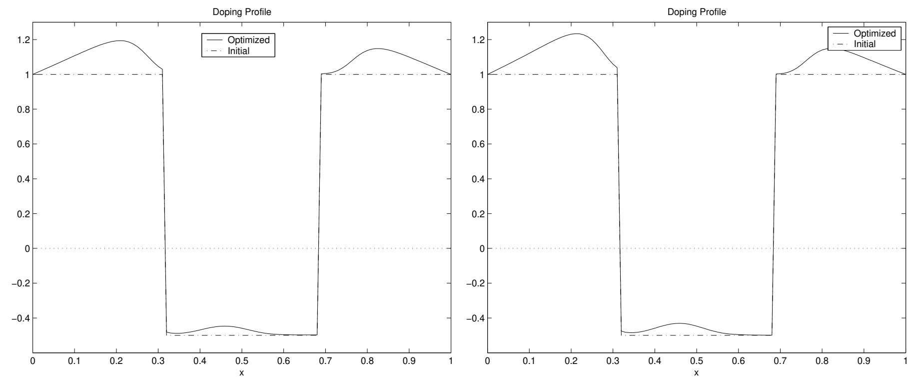

FIG. 5.5. *Initial (dash-dotted) and optimized (solid) doping profile in Example 5.2, for $\epsilon = 10^{-6}$ (left) and $\epsilon = 10^{-8}$ (right).*

intially increases since the doping is pulled away from the initial one. In the later stage of the iteration, the observation part remains almost constant and decrease in the objective functional is obtained only due to (slow) decrease in the energy. An inspection of the current-voltage plot shows that also the optimized doping profile yields a characteristic whose absolute value increases exponentially for positive applied voltages, but lies above the initial one for all applied voltages.

5.2. NPN-Diode. Our second numerical example is a npn-diode, with the same parameter settings as in Example 5.1, and with the same choice of the objective. The initial doping profile is piecewise constant function taking the values one and minus one; it is shown as the dash-dotted function in Figure 5.5. The values of the parameter ϵ that lead useful results are now between 10^{-6} and 10^{-8}, which is due to the lower absolute values of the current obtained in this example. The objective value obtained in the first case is around 0.4, while the objective is reduced almost to zero for the the second one. The evolution of the objective functional, the observation and the energy term is plotted in Figure 5.8, showing a similar behaviour as in Example 5.1. For $\epsilon = 10^{-8}$, the energy term is already negligible and the iteration is driven by the reduction of the observation error.

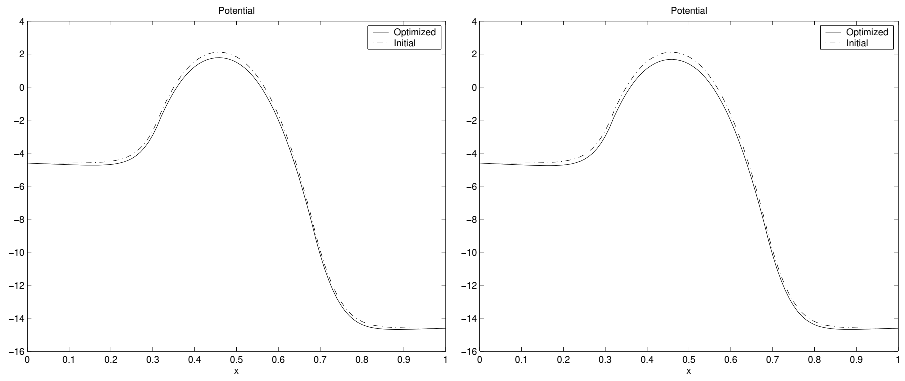

FIG. 5.6. *Initial (dash-dotted) and optimized (solid) potential in Example 5.2, for $\epsilon = 10^{-6}$ (left) and $\epsilon = 10^{-8}$ (right).*

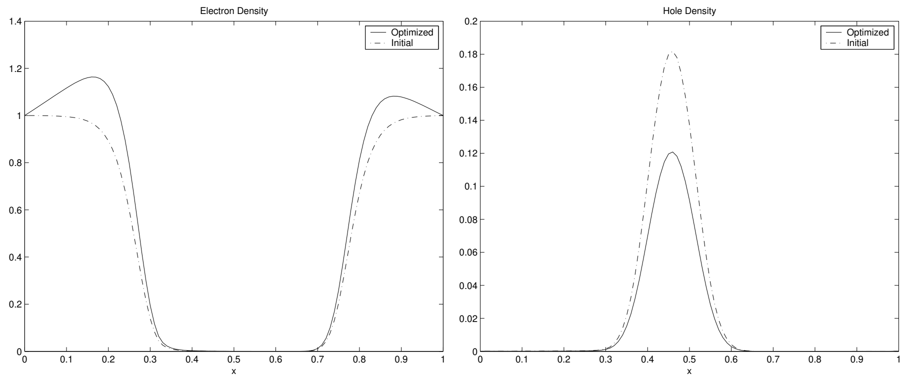

FIG. 5.7. *Initial (dash-dotted) and optimized (solid) electron density (left) and hole density (right) in Example 5.2, for $\epsilon = 10^{-8}$.*

The optimized and initial values for the doping profile are plotted in Figure 5.5 and for the potential in Figure 5.6. In this case, the change in the potential is quite small, and the doping profile is increased slightly both in the n- and p-regions. A more significant change happens in the electron density, shown for the case of $\epsilon = 10^{-8}$ in Figure 5.7. As one might expect, the electron density is changed mainly in the n-regions, while the hole density is changed in the p-region.

Finally, we plot the negative CV-characteristics (i.e., the map $U \mapsto J$) of the initial and optimized device for both values of ϵ. The shape of these current-voltage curves remains similar for all values of ϵ, but obviously changes in magnitude as ϵ tends to zero.

5.3. MESFET Device. As our final example, we consider the optimal design of a metal-semiconductor field-effect transistor (MESFET) in two spatial dimensions. We use a device geometry and an initial doping profile as in an example considered [12], with a length of $6\mu m$ and a width of $2\mu m$. The geometry and the position of the contacts is shown in Figure 5.10. The scaled initial doping profile (by the value $C_s = 10^{14} cm^{-3}$ is shown in Figure 5.11; in order to improve the visibility, we plot the initial values and subsequently the results with different scaling of the x- and

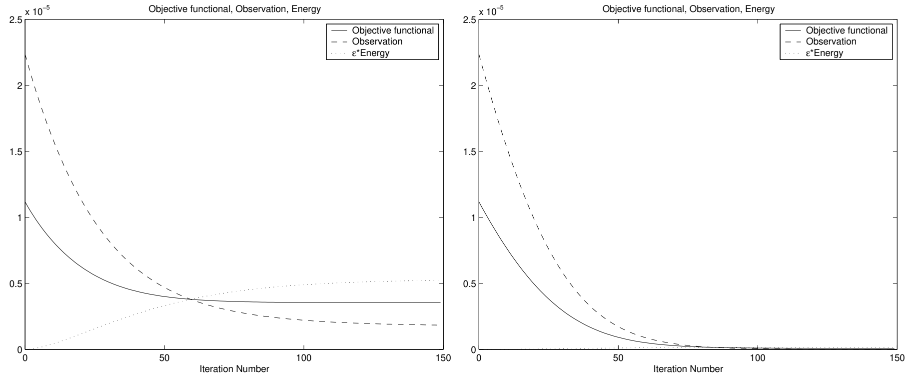

FIG. 5.8. *Evolution of the objective functional (solid), observation (dashed) and energy (dotted) in Example 5.2, for $\epsilon = 10^{-6}$ (left) and $\epsilon = 10^{-8}$ (right).*

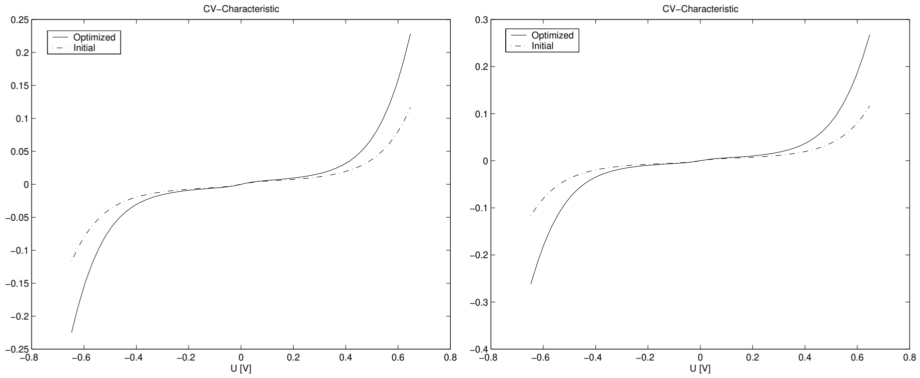

FIG. 5.9. *Negative current-voltage characteristic obtained with the initial (dash-dotted) and the optimized doping profile (solid) in Example 5.2, for $\epsilon = 10^{-6}$ (left) and $\epsilon = 10^{-8}$ (right).*

the y-axis. A MESFET can be modeled as a unipolar device, which is also reflected by the positivity of the doping profile in the whole device region. Thus, we have $p = v = 0$ in Ω and the equation for v as well as the adjoint equation determining the Lagrangian variable $\mu_2 \equiv 0$ can be eliminated, which reduces the computational effort. The boundary data are specified by $n = 0.5(C + \sqrt{C^2 + 4\delta^2})$, a temperature of $T = 300°$ on each contact, and

- at the source: $V = V_{bi} - 0.1[V] = 0.1670[V]$.
- at the drain: $V = V_{bi} + 0.4[V] = 0.6670[V]$.
- at the gate: $V = V_{bi} = 0.2385[V]$.

Our objective is to increase the current flow over the drain by 50%, and consequently we chose

$$I^* = \int_\Gamma J_0 . d\nu, \tag{5.2}$$

where Γ is the drain contact and J_0 is the current flow density obtained with the initial doping.

For the finite element discretization of the original problem we used an adaptive solver, with a resulting mesh (shown in Figure 5.12) consisting of $n_t = 15434$ trian-

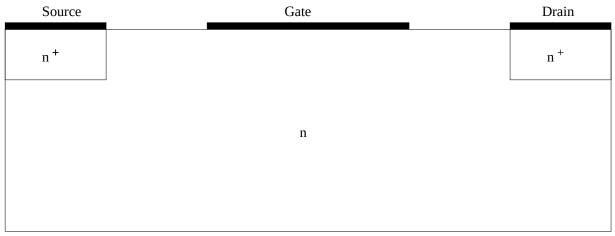

FIG. 5.10. *Device geometry in Example 5.3.*

FIG. 5.11. *Initial value of the doping profile and the potential in Example 5.3.*

gular elements. This mesh is used subsequently also for the optimization algorithm. This strategy of using grid adaption only for the initial problem is motivated by the above observation that steep junctions will remain at the same location during the optimization process.

In this case, it turns out that a suitable choice of ϵ is 10^{-3}, and here we show the results for this value. Changes of ϵ lead to a similar behaviour as in the previous examples. The optimized doping profile and the optimized potential are shown in Figure 5.14. A comparison with the initial value shows that the doping profile is increased mainly close to the drain, while it is even slightly decreased close to the device corner opposite to the drain. The change in the potential is less significant, which is due to the fact that the main shape of the potential is determined by the rather high difference in the boundary values. Changes in the doping profile (and in the electron density $n = e^V u$ are mainly caused by the Laplacian of $V - V^*$, which is still of considerable magnitude.

An inspection of the evolution of the objective demonstrates again the efficiency of our approach, since a minimum is obtained with only few iterations. Since in each iteration, we only have to solve four scalar elliptic partial differential equations, the numerical effort per iteration is similar to two Gummel-type iteration steps for the (unipolar) drift-diffusion system. Since in general the number of iterations in a Gummel-type method for the drift-diffusion system is of similar size than the number of iterations needed for the optimal design problem, the overall numerical effort for optimization is around the effort for two forward solves of the nonlinear drift-diffusion system, which is a surprising result.

6. Conclusions. We have presented a new, fast approach to the optimal design of semiconductor devices, which can be applied if a performance optimization of the device at a single fixed applied voltage is desired. The numerical experiments illustrate reasonable convergence properties of the simple algorithm we have proposed to solve the optimal design problem, and clearly demonstrate its efficiency. In particular, we have obtained an optimization procedure with a numerical effort of similar magnitude as few forward solves.

We finally would also like to mention the natural limitations or possible generalizations of the approach presented in this paper. These limitations arise if the optimization goal involves current flows for several applied voltages and consequently several different potentials, since we can only interpret one of the potentials as the design variable in this case. This statement applies in particular in the context of

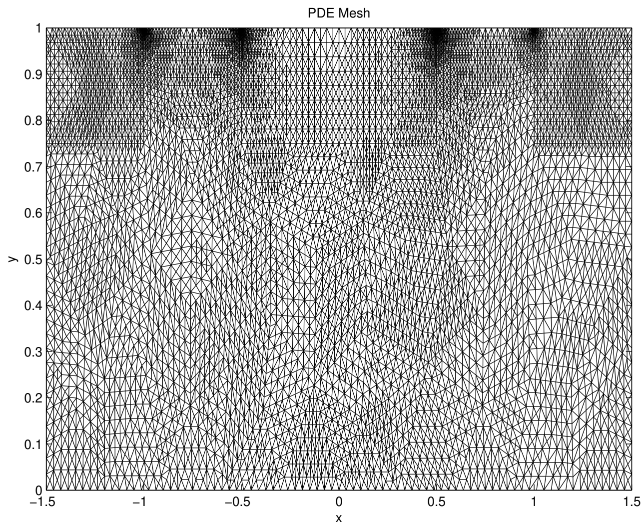

FIG. 5.12. *Mesh used for the optimization in Example 5.3.*

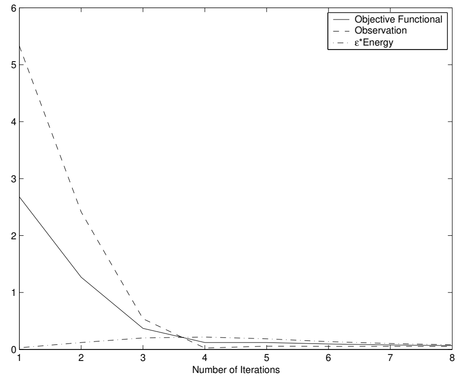

FIG. 5.13. *Evolution of the objective functional (solid), observation error (dashed) and the energy term (dash-dotted) in Example 5.3.*

identifying unknown doping profiles, which is usually done by minimizing a least-squares functional involving a large number of different voltages (cf. [2]). In many typical optimal design situations however, the aim is to control at most the currents for two-different voltages, namely for an *on-state voltage* and an *off-state voltage* (close to equilibrium). The usual aim in such a situation is to maximize the on-state current flow on a contact by keeping the off-state current flow below some threshold value. In optimal design problems of this type it seems natural to eliminate the on-state potential, since solutions of the drift-diffusion system close to equilibrium are rather cheap. A numerical investigation of such optimal design situations shall be left to future research.

Acknowledgements. The authors thank Prof. Peter Markowich (University of Vienna) for interesting discussions and in particular for stimulating this collaboration. Financial support is acknowledged by the Austrian Science Foundation FWF und project SFB F 013 / 08, and by the European Union under research network *Hyperbolic*

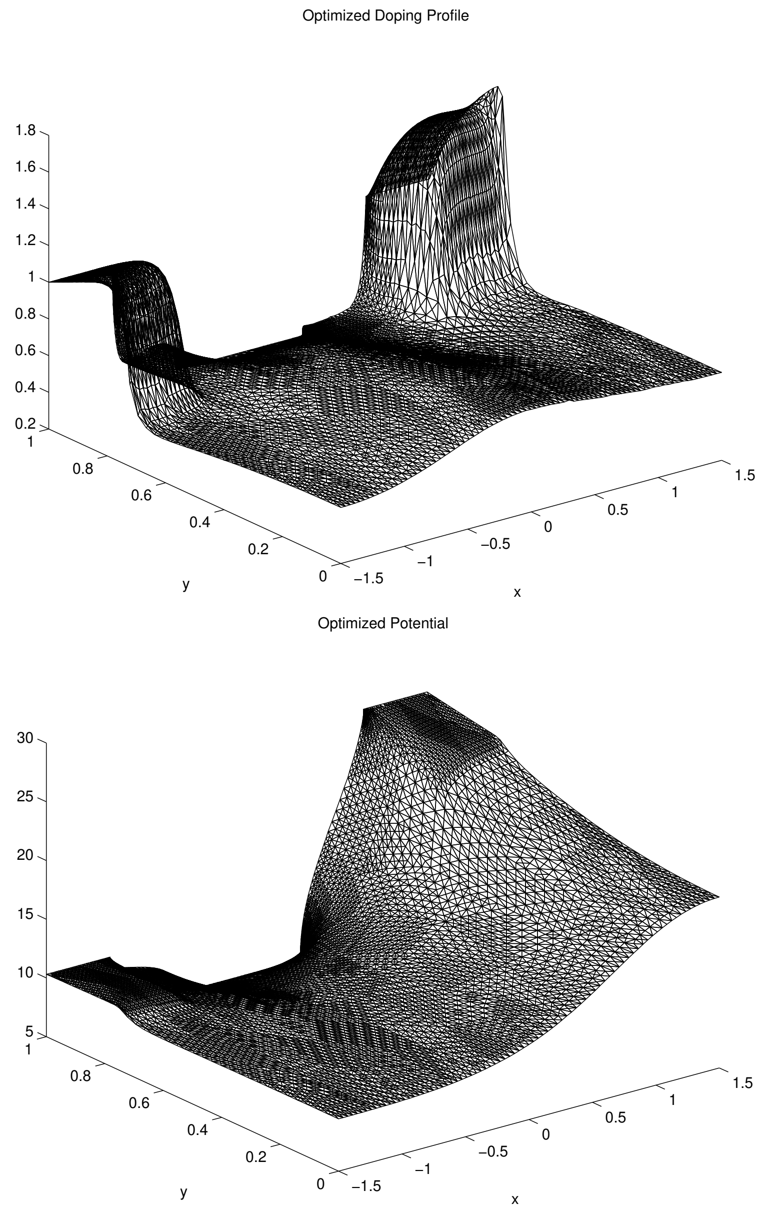

FIG. 5.14. *Optimized doping profile and potential in Example 5.3,* $\epsilon = 10^{-3}$.

and Kinetic Equations, contract HPRN-CT-2002-00282.

REFERENCES

[1] F.Brezzi, L.D.Marini, P.Pietra *Two-dimensional exponential fitting and applications in drift-diffusion models*, SIAM J. Numer. Anal., **26** (1989), pp. 1342-1355.

[2] M.Burger, H.W.Engl, P.Markowich, P.Pietra, *Identification of doping profiles in semiconductor devices*, Inverse Problems, **17** (2001), pp. 1765-1795.

[3] M.Burger, H.W.Engl, P.Markowich, *Inverse doping problems for semiconductor devices*, in:

T.F.Chan, Y. Huang, T.Tang, J.A.Xu, L.A.Ying, eds., *Recent Progress in Computational and Applied PDEs*, Kluwer, Boston, Dordrecht, London, 2002, pp. 39-54.

[4] M.Burger, R.Pinnau, *Exponential fitting for adjoint equations in semiconductor design* (2002), in preparation.

[5] L.Ciampolini, *Scanning capacitance microscope imaging and modelling*, PhD Thesis, ETH Zürich, Hartung-Gorre Verlag, Konstanz, 2001.

[6] A.C.Diebold, M.R.Kump, J.J.Kopanski, D.G.Seiler, *Characterization of two-dimensional dopant profiles: status and review*, J. Vac. Sci. Technol. B, **14** (1996), pp. 196-201.

[7] W.Fang, E.Cumberbatch, *Inverse problems for metal oxide semiconductor field-effect transistor contact resistivity*, SIAM J. Appl. Math., **52** (1992), pp. 699-709.

[8] Fang, K.Ito, *Identifiability of semiconductor defects from LBIC images*, SIAM J. Appl. Math., **52** (1992), pp. 1611-1626.

[9] Fang, K.Ito, *Reconstruction of semiconductor doping profile from laser-beam-induced current image*, SIAM J. Appl. Math., **54** (1994), pp. 1067-1082.

[10] M.Hinze, R.Pinnau, *Optimal control of the drift-diffusion model for semiconductor devices*, in: K.-H.Hoffmann, I.Lasiecka, G.Leugering, and J.Sprekels, editors, *Optimal Control of Complex Structures*, volume 139 of *ISNM*, Birkhäuser, 2001, pp. 95-106.

[11] M.Hinze, R.Pinnau, *An optimal control approach to semiconductor design*, Math. Mod. Meth. Appl. Sci., **12** (2002), pp. 89-107.

[12] S.Holst, A.Jüngel, P.Pietra, *A mixed finite-element discretization of the energy-transport model for semiconductors*, to appear in SIAM J. Sci. Comp.

[13] N.Khalil, *ULSI characterization with technology computer-aided design*, PhD-Thesis, Technical University Vienna, 1995.

[14] N.Khalil, J.Faricelli, D.Bell, S.Selberherr, *The extraction of two-dimensional MOS transistor doping via inverse modeling*, IEEE Electron Device Lett., **16** (1995), pp. 17-19.

[15] P.A.Markowich, *The Stationary Semiconductor Device Equations*, Springer, Wien, New York, 1986.

[16] P.A.Markowich, C.A.Ringhofer, C.Schmeiser, *Semiconductor Equations*, Springer, Wien, New York, 1990.

[17] M.S.Mock. *Analysis of Mathematical Models of Semiconductor Devices*, Boole Press, Dublin, first edition, 1983.

[18] R.Plasun, M.Stockinger, R.Strasser, S.Selberherr, *Simulation based optimization environment and its application to semiconductor devices*, in: Proceedings IASTED Intl. Conf. on Applied Modelling and Simulation, 1998, pp. 313-316.

[19] S.Selberherr, *Analysis and Simulation of Semiconductor Devices*, Springer, Wien, New York, 1984.

[20] M. Stockinger, *Optimization of ultra-low-power CMOS transistors*, PhD Thesis, Technical University Vienna, 2000.

[21] M.Stockinger, R.Strasser, R.Plasun, A.Wild, S.Selberherr, *A Qualitative Study on Optimized MOSFET Doping Profiles*, in: Proceedings SISPAD 98 Conf., Leuven, 1998, pp. 77-80.

[22] M.Stockinger, R.Strasser, R.Plasun, A.Wild, S.Selberherr, *Closed-loop MOSFET doping profile optimization for portable systems*, in: Proceedings Intl. Conf. on Modeling and Simulation of Microsystems, Semiconductors, Sensors, and Actuators, San Juan, 1999, pp. 411-414.

[23] W.R. Van Roosbroeck, *Theory of flow of electrons and holes in germanium and other semiconductors*, Bell Syst. Tech. J., **29**, (1950), pp. 560-607.